Available online at www.sciencedirect.com
SCIENCE DIRECT®
Journal of Catalysis 231 (2005) 365–380
JOURNAL OF CATALYSIS
www.elsevier.com/locate/jcat

Structure and reactivity in the selective oxidation of methane to formaldehyde of low-loaded FeO_x/SiO_2 catalysts

Francesco Arena [a,*], Giorgio Gatti [b], Gianmario Martra [b], Salvatore Coluccia [b], Lorenzo Stievano [c], Lorenzo Spadaro [d], Pio Famulari [a], Adolfo Parmaliana [a]

[a] *Dipartimento di Chimica Industriale e Ingegneria dei Materiali, Università degli Studi di Messina, Salita Sperone 31, 98166 S. Agata (Messina), Italy*
[b] *Dipartimento di Chimica IFM and NIS Centre of Excellence, Università di Torino, Via P. Giuria 7, 10125 Torino, Italy – UdR TO1 of INCA Interuniversity Consortium*
[c] *Laboratoire de Réactivité de Surface, Université Paris VI, UMR 7609, Place Jussieu 4, 75252 Paris, France*
[d] *Instituto CNR-ITAE "Nicola Giordano", Salita S. Lucia 39, I-98126 S. Lucia (Messina), Italy*

Received 6 December 2004; revised 20 January 2005; accepted 24 January 2005

Available online 23 March 2005

Abstract

The structure of low-loaded (0.09–0.73 Fe wt%) FeO_x/SiO_2 catalysts prepared by *adsorption–precipitation* of Fe^{2+} precursor on silica (AP) has been assessed by DR UV–Vis and Mössbauer techniques in comparison with counterpart *incipient wetness* (IW) systems. Spectroscopic findings indicate the *speciation* of the active phase into *isolated* Fe^{3+} *species*, *oligomeric 2-d* FeO_x *patches*, and *3-d* Fe_2O_3 *nanoparticles*, characterised by decreasing interaction strength with silica carrier. The reduction pattern of the above surface structures has been probed by temperature-programmed reduction (TPR) measurements, and a deconvolution analysis of spectra allowed the concentration of the various surface species to be highlighted. The catalytic activity in the *selective oxidation of* CH_4 *to HCHO* with oxygen (MPO) has been systematically evaluated by batch (BR) and continuous-flow (CF) measurements in the range of 400–750 °C. Direct relationships among Fe dispersion and specific atomic rate of CH_4 conversion (Fe_{CH_4}, s^{-1}) and HCHO formation (Fe_{HCHO}, s^{-1}) confirm the superior catalytic performance of AP systems. After a poor reactivity of "*isolated species*" and the unselective behaviour of *3-d* Fe_2O_3 particles, *2-d* oligomeric *patches* feature the best catalytic pattern, owing to an optimum Fe–O bond strength. Sintering and surface reconstructuring phenomena affect the catalyst stability during the MPO reaction.

Keywords: FeO_x/SiO_2 catalysts; Methane partial oxidation; Formaldehyde; Preparation method; Fe precursor; Deconvolution analysis; Surface structures; Redox properties; Fe dispersion; Sintering

1. Introduction

The direct conversion of natural gas (NG) streams into commodity chemical products actually constitutes one of the hottest topics in catalysis, since potential process routes employing novel catalytic approaches in combination with low-cost feedstocks could result in significant economic advantages over current technologies [1,2]. Despite the proposal of many catalysts for the selective oxy-functionalisation of C_1–C_5 alkanes in both the scientific and patent literature [1–12], a low process productivity still remains the most significant shortcoming for industrial exploitation [1–5]. Furthermore, the partial oxidation of methane to oxygenates does not obey some rules for the selective activation of C_2–C_5 alkanes [1–5].

Several studies in recent years have indicated a superior functionality of FeO_x/SiO_2 catalysts in the partial oxidation of methane to formaldehyde (MPO), though it has been argued that the structure of Fe^{3+} centres determines their activity–selectivity pattern [6–11]. Specifically, "isolated" Fe^{3+} moieties assist selective oxidation paths leading

* Corresponding author.
E-mail address: francesco.arena@unime.it (F. Arena).

0021-9517/$ – see front matter © 2005 Published by Elsevier Inc.
doi:10.1016/j.jcat.2005.01.029

to oxygenated products, whereas Fe_2O_3 aggregates and/or (nano)particles mostly yield CO_x because of a high availability of lattice oxygen ions driving the further oxidation of intermediates [6–11]. Then in addition to catalyst formulations involving silica as a carrier of transition-metal ions (Mo, V, Fe, etc.) [3–9,12–14], stoichiometric compounds such as $Fe_2(MoO_4)_3$ and $FePO_4$, in which the counteranion acts as a "spacer" for "isolation" of the active Fe^{3+} redox centres, were also found to be effective catalysts for the oxy-functionalisation of CH_4 [4,15]. In fact, both theoretical considerations [2,12] and experimental findings [1–12,15–18] convey that a proper catalyst design must ensure a high dispersion (e.g., "site isolation") of suitable transition-metal ions (e.g., V, Mo, Fe) over a matrix featuring a weak Brønsted-type acidity.

Furthermore, previous studies of the catalyst steady state by reaction temperature O_2 chemisorption measurements (RTOC) allowed the mechanism and kinetics of the MPO on silica-based catalysts to be highlighted [2,12,19–21]. According to recognised principles of oxidation catalysis [2,12,16] and ab initio calculations of the energetic barrier for CH_4 activation on the FeO^+ complex [17,18], we developed a formal kinetic model describing in detail the steady-state conditions and the activity-selectivity pattern of low-loaded FeO_x/SiO_2 catalysts [2,12,19–21]. Because of the second-order dependence of CH_4 conversion and a first-order inverse dependence of HCHO selectivity on concentration of active sites, respectively [2,12,21], we pointed out that process productivity (STY) can be enhanced by a rise in the dispersion of Fe^{3+} ions across a silica matrix, leading to the exploitation of alternative synthesis routes [2,9–12].

The physico-chemical and catalytic properties [22–32] of supported iron oxide systems have been widely investigated, and a peculiar reactivity has generally been documented concomitantly with a high dispersion of the active phase [8,23,28,30,31]. A high, although selective, catalytic functionality of FeO_x-supported systems has been found in the SCR of NO_x [23,25], in the selective oxidation of benzene to phenol [31] and ethylbenzene to styrene [32]. That close relationship between the structure and reactivity of the active phase compelled the adoption of special preparation methods, such as ion exchange [22–24,26–29] and CVD [25,26,28], to attain a homogeneous dispersion of Fe^{3+} ions mostly across zeolite-type matrices.

Therefore, this paper highlights the reliability of the "adsorption–precipitation" route (AP) [2,9–12] in promoting the dispersion of *low-loaded* (150–7300 ppm Fe) FeO_x/SiO_2 catalysts. A basic assessment of the effects of preparation route and Fe loading on the *speciation* and redox features of the active phase makes it possible to predict in a detailed way the catalytic pattern of low-loaded FeO_x/SiO_2 systems in MPO according to the density, structure, and reactivity of surface FeO_x species. The catalytic efficiency of the various surface structures and the occurrence of catalyst *deactivation phenomena* are also discussed.

2. Experimental

2.1. Materials

2.1.1. Catalysts

Two commercial "precipitated" SiO_2 samples, F5 and Si 4-5P (Akzo Nobel), were used for the preparation of several FeO_x/SiO_2 catalysts by "incipient wetness" (IW) and "adsorption–precipitation" (AP) routes, respectively. The former were obtained by stepwise addition of $Fe(NO_3)_3$ aqueous solutions (pH $\sim$2.5) to powder silica carriers, and AP systems were prepared according to the following procedure [2,9–12]. An aqueous suspension of powder silica, put into a three-necked bottle, was kept at room temperature under continuous nitrogen flow ($\sim$100 STP $cm^3\,min^{-1}$) and stirring ($\sim$600 rpm) to remove oxygen, avoiding any further air admission. Then, an amount of $FeSO_4$ corresponding to the designed Fe loading was added to the suspension, the pH of which was gradually raised to 7–8 by dropwise addition of a concentrated NH_4OH solution. The suspension was kept at the final pH value (with stirring and N_2 bubbling) for 1 h, during which the quantitative adsorption (> 98%) of Fe^{II} ions was attained. Afterwards, the solid was filtered and repeatedly washed with bi-distilled water.

Two aliquots of F5 (S1) and Si 4-5P (S2) silica were subjected to the above impregnation steps without any Fe precursors in the solution, to obtain respective "blank" samples.

All of the samples were dried at 100 °C and then calcined at 600 °C for 6 h in air. A list of samples, along with the relative preparation methods, Fe loading (wt ppm), BET surface area value (SA_{BET}, m^2/g), and specific surface loading (SSL, $Fe_{at}\,nm^{-2}$), are given in Table 1. Sample designations (F[xxxx]Sy-zz) take into account the silica carrier (S1 or S2), Fe loading [wt ppm], and preparation method (F[xxxx]Sy-IW and F[xxxx]Sy-AP), referred to as IW and AP routes, respectively.

2.2. Methods

UV–Vis diffuse reflectance (DR UV–Vis) spectroscopy measurements were performed on fine powders of the samples put into a cell with optical quartz walls, permanently connected to a vacuum line (residual pressure: 1.0×10^{-6} Torr; 1 Torr = 133.33 Pa). The spectra were collected with a Perkin-Elmer Lambda 900 instrument equipped with an integrating sphere and Ultra-White Teflon as a reference material.

Mössbauer ^{57}Fe spectra were recorded at room temperature (20 °C) and at liquid He temperature (−269 °C) with both the $^{57}Co/Rh$ source and absorber at the same temperature. The spectrometer was operated with a sinusoidal velocity waveform, and the spectra were fitted by superimposition of appropriate sets of Lorentzian lines, with the use of MOS-90 PC software [33]. In the case of a magnetic

Table 1
List of the studied catalysts

Code	Support	Preparation method	Fe loading (wt ppm)	SA_{BET} ($m^2\ g^{-1}$)	SSL ($Fe_{at}\ nm^{-2}$) $\times 10^2$
S1	F5	–	150	607	0.27
S2	Si 4-5P	–	200	385	0.56
F[1000]S1-IW	F5	IW–Fe^{III}	1000	593	1.8
F[1000]S2-IW	Si 4-5P	IW–Fe^{III}	1000	402	2.7
F[4200]S1-IW	F5	IW–Fe^{III}	4200	586	7.7
F[4300]S2-IW	Si 4-5P	IW–Fe^{III}	4300	388	11.9
F[3700]S2-AP	Si 4-5P	AP–Fe^{II}	3300	399	10.0
F[1000]S1-AP	F5	AP–Fe^{II}	1000	601	1.8
F[1300]S1-AP	F5	AP–Fe^{II}	1300	599	2.3
F[3700]S1-AP	F5	AP–Fe^{II}	3700	597	6.7
F[5900]S1-AP	F5	AP–Fe^{II}	5900	592	10.8
F[7300]S1-AP	F5	AP–Fe^{II}	7300	581	13.5

sextet, an asymmetric Gaussian distribution of the hyperfine field was allowed for. The resulting parameters, such as average magnetic hyperfine field B_{hf}, electric quadrupole splitting QS, isomer shift IS (relative to α-Fe_2O_3), Lorentzian linewidth (LW), and resonance area, A, as a percentage of the Fe content, are taken into account.

Temperature-programmed reduction (TPR) analysis was performed with a linear quartz microreactor (i.d. 4 mm) fed with a 6% H_2/Ar reducing mixture flowing at 30 STP $cm^3\ min^{-1}$, timely purified of any O_2 and H_2O. Measurements were carried out in the range of 200–800 °C with a heating rate of 20 °C min^{-1}, with an amount of catalyst corresponding to an Fe load of ca. 0.2 mg, to ensure differential H_2 consumption rates. Before measurements all the catalyst samples were treated in situ at 600 °C for 30 min under a 10% O_2/He flow. The H_2 consumption was monitored by a TCD connected by a ChromCard (**Fisons Instruments**) to a PC for data storage and processing, and the response was quantitatively calibrated from the TPR area of known amounts of CuO. Under such conditions, TPR data were reproducible in terms of both peak maximum position (±10 °C) and extent of hydrogen consumption (±10%).

Modelling of TPR spectra has been performed by deconvolution analysis of experimental profiles by a linear combination of Gaussian components [34–36], with the use of the "PeakFit" software package (Jandel Scientific).

Catalyst testing in the MPO under differential conversion conditions was performed with a "recirculation batch reactor" (BR) operating at 650 °C and 1.71 bar [8,9,19,20], at a total flow rate of 1000 STP $cm^3\ min^{-1}$ ($He:N_2:CH_4:O_2 = 6:1:2:1$) and with a catalyst sample of 0.05 g, unless otherwise specified.

The performance of FeO_x/SiO_2 catalysts has been also evaluated under integral conversion conditions by continuous-flow (CF) temperature-programmed catalytic reaction tests in the range of 400–750 °C [13], with the use of a quartz micro-reactor (i.d. 4 mm) containing 0.05 g of catalyst fed with a reaction mixture (CH_4, 20%; O_2, 10%; He, 70%) flowing at 50 STP $cm^3\ min^{-1}$, unless otherwise specified. The temperature was ramped at rate of 10 °C min^{-1}, enabling a continuous scanning of reaction stream with a quadrupole mass spectrometer (Thermolab, Fisons Instruments) connected to the reactor by a heated (180 °C) inlet capillary system [13].

3. Results

3.1. Characterisation of the "fresh" catalysts

3.1.1. DR UV–Vis spectroscopy

The first, though qualitative, evidence of the rather different efficiencies of the employed preparation routes in promoting the iron dispersion on silica carriers stems from the different colours of the AP and IW catalysts. Whereas a typical brownish dye of the former signals the presence of Fe_2O_3 aggregates at any loading (0.1–0.43 wt% Fe), AP samples look colourless up to a loading of 0.73 wt% (F[7300]S1-AP). However, a basic evaluation of the iron dispersion on the various catalysts can be made on the basis of the DR UV–Vis spectra of the calcined samples outgassed at room temperature (room temperature) (shown in Fig. 1). Under such conditions Fe ions are expected to have an octahedral coordination (e.g., six ligands corresponding to oxygen atoms of the support and adsorbed water/hydroxyls), and, after the calcination at 600 °C, their ON must be +3 [27–30].

DR UV–Vis spectra for the bare S2 (a) and S1 (a′) supports are shown in Fig. 1A, including also the spectra of the F[1000]S2-IW (b), F[4300]S2-IW (c), and F[4200]S1-IW (d) catalysts. In the case of the silica support, a main band at 42,500 cm^{-1}, two weaker and overlapped components at 36,500 and 32,500 cm^{-1}, and a broad tail spanning the 30,000–15,000 cm^{-1} range, are observed (Fig. 1A, spectrum a). These absorptions can be attributed to charge transfer (CT) transitions involving titanium and iron ions contained as impurities [27,37]. Both isolated Ti^{4+} and Fe^{3+} in (distorted) tetrahedral coordination located in the SiO_2 bulk could be responsible for the main signal at 42,500 cm^{-1} [27,37]. Notably, isolated Fe^{3+} ions in a (distorted) octa-

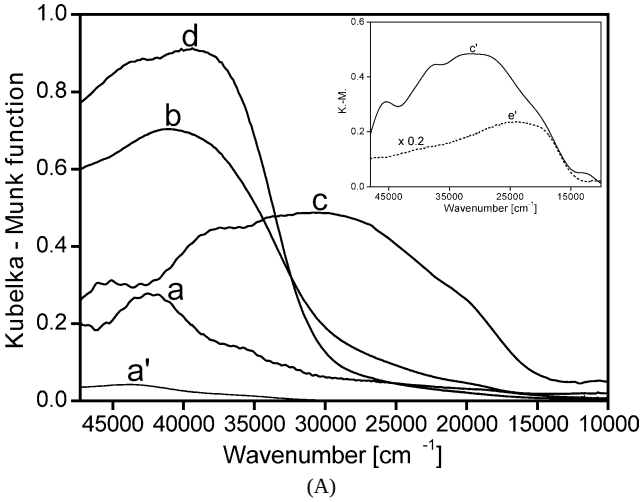

(A)

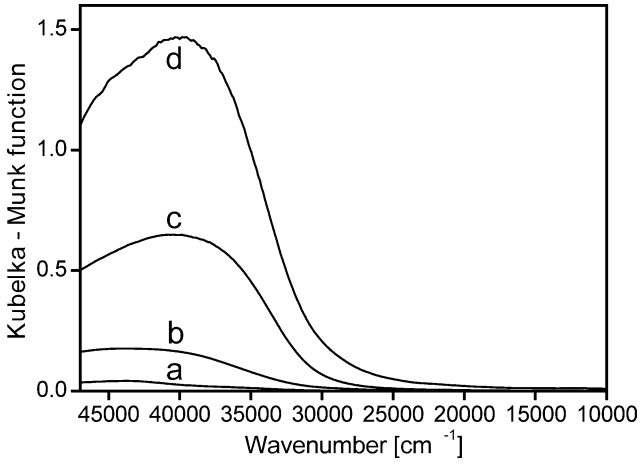

(B)

Fig. 1. (A) DR UV–Vis absorption spectra of: (a) bare S2 silica; (b) F[1000]S2-IW; (c) F[4300]S2-IW; and (d) F[4200]S1-IW samples. For comparison also the spectrum of the S1 silica (a′) is included. (B) DR UV–Vis spectra of: (a) S1; (b) F[1000]S1-AP; (c) F[3700]S1-AP; and (d) F[7300]S1-AP samples. *All the samples have been outgassed at room temperature for 1 h.*

hedral symmetry at the surface of silica particles, where they can expand their ligand sphere by adsorbing water molecules, can also contribute significantly to this band, presenting a partner component at 36,500 cm^{-1} [38]. This latter absorption, however, might also be a monitor of the presence of surface isolated Ti^{4+} ions in (distorted) octahedral coordination [39]. Finally, the shoulder at 32,500 cm^{-1} and the lower frequency tail can be attributed to TiO_x and FeO_x aggregates, ranging from "cluster-like" species to nanoparticles; the corresponding electronic absorption decreases in energy as their size increases [40].

For the F[1000]S2-IW sample, the overall absorption intensity increases ca. 2.5 times, and the spectral profile is dominated by a broad band with a maximum at 41,000 cm^{-1}, which is asymmetric on the lower frequency side and is accompanied by a weak tail in the range of 30,000–15,000 cm^{-1} (Fig. 1A, spectrum b). The main component at 41,000 cm^{-1} is assignable to the most intense CT band of isolated Fe^{3+} ions in octahedral coordination (the six ligands are oxygen atoms of the support and adsorbed water molecules/hydroxyls), with an associated weaker partner in the 37,000–35,000 cm^{-1} range [38,41]. The remaining part of the absorption profile at lower frequency reveals the presence of Fe^{3+} species in the form of oxidic dimers/oligomers (38,000–25,000 cm^{-1}) and 3-d Fe_2O_3 particles (25,000–10,000 cm^{-1}) [27,42].

The components related to isolated Fe^{3+} species appear to be strongly reduced in intensity in the spectrum of the F[4300]S2-IW sample, whereas the intensity of absorptions due to aggregated species is significantly enhanced, thus becoming the dominant feature (Fig. 1A, spectrum c). The heavy shoulder at ca. 20,000 cm^{-1} monitors the massive presence of nanometric Fe_2O_3 particles, after the spectrum of a silica-diluted hematite powder with an average particle size of 3 nm (Fig. 1A; see inset). A corresponding decrease in absorption due to isolated species indicates that the addition of large amounts of Fe by IW involves a high degree of agglomeration of Fe^{3+} ions.

The effect of the specific surface area of the silica carrier on dispersion of the iron species can be assessed by a comparison of the spectra of the similarly loaded F[4300]S2-IW (Fig. 1A, spectrum c) and F[4200]S1-IW (Fig. 1A, spectrum d) system. With respect to catalyst supported on S2, the F[4200]S1-IW sample exhibits a spectrum dominated by a complex absorption with maxima at 43,000 and 39,000 cm^{-1}, resulting from overlapping components of isolated octahedral Fe^{3+} species and octahedral Fe^{3+} species in the form of oxidic dimers/oligomers, indicating a better dispersion of iron in this case.

For the differently loaded catalysts prepared via the AP method on S1 silica (Fig. 1B), the DR UV–Vis patterns appear in any case to be dominated by a main component located at a frequency higher than 40,000 cm^{-1}, even for a Fe loading of 0.73 wt% (Fig. 1B, spectrum d). This indicates that well-dispersed Fe^{3+} ions in an octahedral coordination are present on such systems. However, a regular shift of the absorption maximum from ca. 45,000 to 40,500 cm^{-1} signals a rising degree of nuclearity of the iron species as the loading increases.

3.1.2. ^{57}Fe Mössbauer spectroscopy

The ^{57}Fe Mössbauer spectra of the F[4300]S2-IW (A) and F[7300]S1-AP (B) samples at room temperature (spectrum a) and at liquid helium temperature (spectrum b) are shown in Fig. 2, and the related parameters are summarised in Table 2. In the case of the Fe[4300]S2-IW sample, the spectrum at room temperature exhibits a simple quadrupole doublet with hyperfine parameters typical of trivalent paramagnetic iron ions in a slightly distorted octahedral environment (Fig. 2A, a), which is transformed almost completely into a six-line pattern at −269 °C (Fig. 2A, b), indicating that almost all of the iron is present in the form of superparamagnetic iron oxide nanoparticles with an average size of ca. 8 nm [43]. Although the hyperfine parameters of

Table 2
Mössbauer parameters of the F[4300]S2-IW and F[7300]S1-AP catalysts

Sample	T (°C)	B_{hf} (T)	QS (mm/s)	IS (mm/s)	LW (mm/s)	A (%)	Iron species (at −269 °C)
F[4300]S2-IW	20	–	0.78 (1)	0.33 (1)	0.52 (1)	100	
	−269	48.1 (1)	−0.02 (1)	0.33 (1)	–	96 (2)	Iron oxide
		–	1.08 (8)	0.39 (1)	0.43 (8)	4 (2)	Paramagnetic Fe^{3+}
F[7300]S1-AP	20	–	0.78 (5)	0.32 (3)	0.51 (1)	40 (20)	
		–	1.08 (5)	0.38 (2)	0.82 (5)	60 (20)	
	−269	39.7 (2)	−0.01 (3)	0.32 (2)	–	52 (5)	Iron oxide
		–	0.99 (1)	0.39 (1)	0.82 (1)	48 (5)	Paramagnetic Fe^{3+}

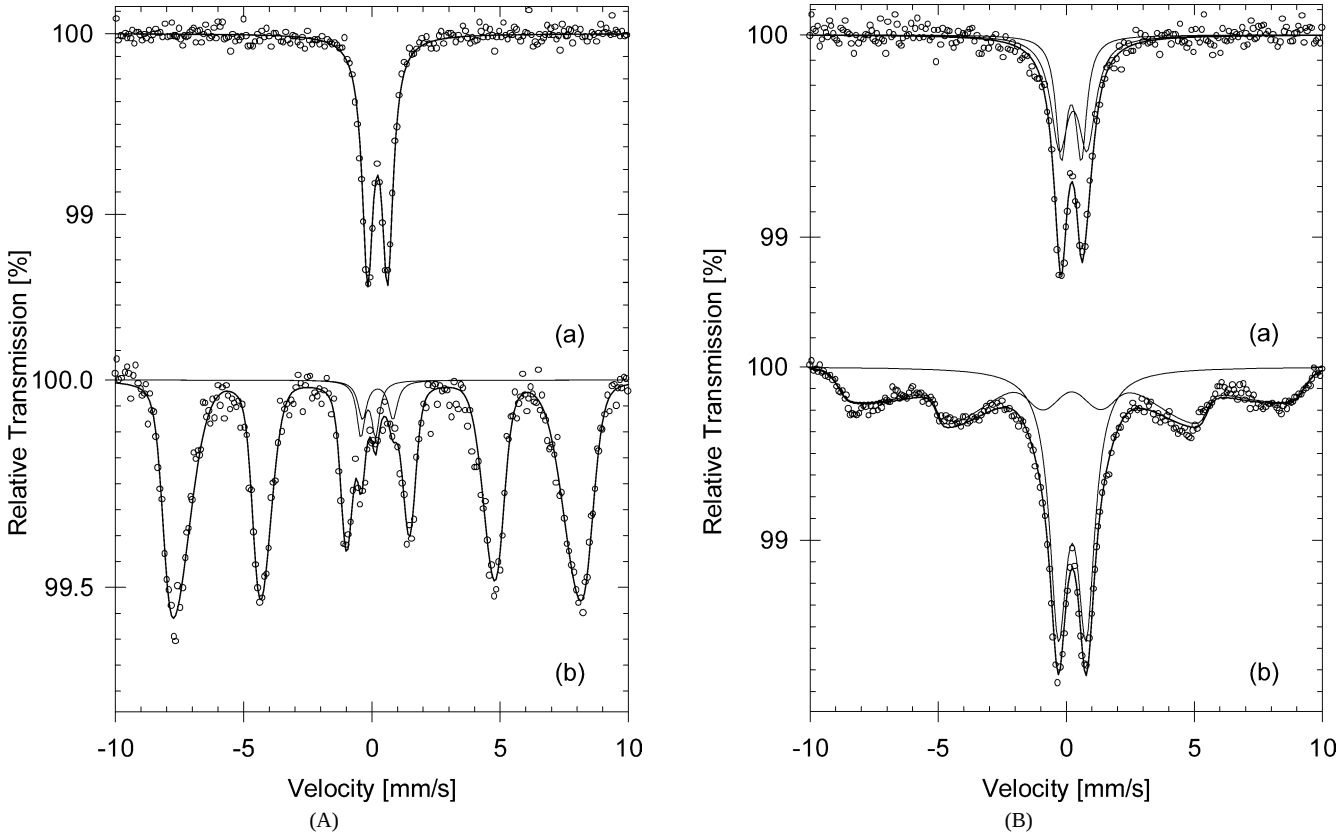

Fig. 2. ^{57}Fe Mössbauer spectra at room temperature (spectra a) and −269 °C (spectra b) of F[4300]S2-IW (A) and F[7300]S1-AP (B) catalysts. *All the samples have been outgassed at room temperature for 1 h.*

this magnetic sextet are slightly different from those of bulk crystalline α-Fe_2O_3 [44], previous studies on FeO_x/SiO_2 systems, bearing a higher Fe loading, suggest that this discrepancy could result either from the nano-size of the α-Fe_2O_3 crystals or from an amorphous character of Fe_2O_3 particles [45].

The spectrum at room temperature of the Fe[7300]S1-AP sample consists of an asymmetric quadrupole doublet, which can be fitted with two Fe(III) components with different QS (Fig. 2B, a), as shown in Table 2. At −269 °C, the coexistence of a quadrupole doublet and a magnetic pattern is observed (Fig. 2B, b). In particular, the resonance area of the magnetic component corresponds to ca. 50% of the overall spectrum, indicating that only about half of the iron content is in the form of superparamagnetic iron oxide species.

3.1.3. Temperature-programmed reduction

TPR profiles (normalised to the integral peak area) of differently loaded FeO_x/SiO_2 catalysts, prepared by AP or IW methods on both F5 and Si 4-5P silicas, are comparatively shown in Fig. 3. Quantitative hydrogen consumption data, expressed as the number of H_2 molecules consumed per Fe atom (H_2/Fe), signal in any case a H_2/Fe ratio close to 0.5 (e.g., 0.42–0.56), thus denoting a "strong" inhibiting effect of the matrix on the reduction of Fe^{2+} ions to Fe^0.

The influence of the Fe loading on the reduction pattern of F[xxxx]S1-AP catalysts is shown in Fig. 3A. The bare S1

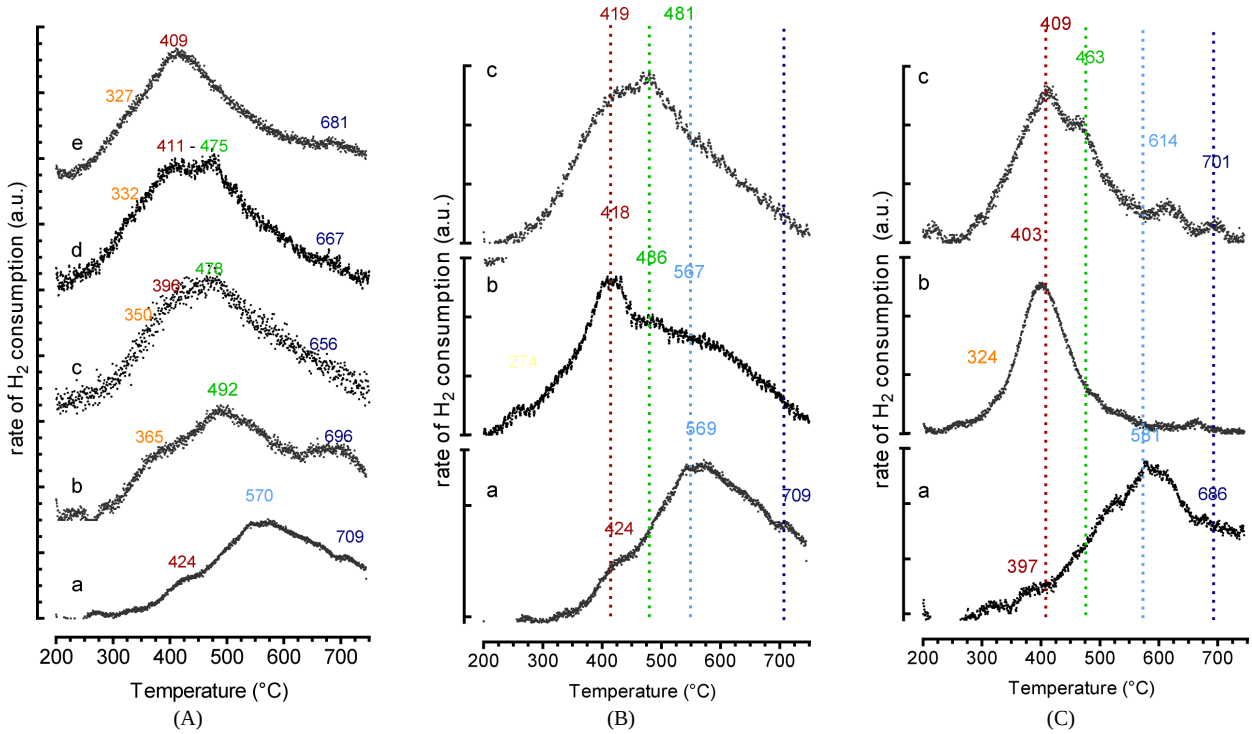

Fig. 3. TPR profiles of (A) F[xxxx]S1-AP catalysts; (B) S1 silica (a); F[4200]S1-IW (b); and F[3700]S1-AP (c); and (C) S2 silica (a); F[4300]S2-IW (b); and F[3700]S2-AP catalysts. *All the spectra are normalised with reference to the integral peak area.*

silica sample (Fig. 3A, a) features a TPR profile spanning the range of 400–800 °C, which accounts for the reduction of Fe^{3+} "impurities" (150 ppm) to Fe^{2+}. From a qualitative point of view, a main reduction peak with a broad maximum at ca. 570 °C dominates such a spectrum, with other weakly resolved maxima at ca. 400 and 700 °C also present. The addition of ca. 0.08% Fe by AP (F[1000]S1-AP) yields a rise in the reduction kinetics at $T < 600$ °C and the appearance of two resolved maxima at 365 and 490 °C. At higher Fe loadings, the reduction profiles of the FeO_x/SiO_2 catalysts retain the qualitative features of the previous system, though peak maxima shift further to lower T. At the highest Fe loading (0.73 wt%), the TPR spectrum of the F[7300]S1-AP sample displays one broad asymmetric peak centred at 409 °C with a tail of H_2 consumption on the high-temperature side, pointing to the presence of several unresolved components in the range of 500–800 °C.

The effects of the preparation method and silica carrier on the reduction pattern of similarly loaded (0.37–0.43 wt%) FeO_x/SiO_2 catalysts are illustrated in Figs. 3B and C, comparing the TPR profiles of F[3700]S1-AP (b) and F[4200]S1-IW (c) samples (Fig. 3B) with those of counterpart F[3700]S2-AP (b) and F[4300]S2-IW (c) samples (Fig. 3C). Like the similar Fe loading (Table 1), the S2 silica (Fig. 3C, a) features a reduction pattern analogous to that of the S1 carrier (Fig. 3B, a), also resulting in a H_2/Fe ratio close to 0.5. As a rule, IW catalysts (Figs. 3B and C, profiles b) display an enhanced reduction rate at lower temperature with respect to similarly loaded F[3700]S1-AP and F[3700]S2-AP (Figs. 3B and C, profiles c), whereas, in comparison, the rate of H_2 consumption at $T > 500$ °C of samples based on S1 silica is systematically higher than that of counterpart S2, indicating some influence of the silica support on the reduction of the active phase, mostly at loadings higher than 0.1 wt%.

3.2. Catalyst testing

3.2.1. BR activity data

The effects of the preparation method and Fe loading on the MPO performance of FeO_x/SiO_2 catalysts have been evaluated by isothermal (650 °C) BR tests at differential conversion per pass conditions (τ, 3.3×10^{-3} s). Activity data, with reference to S1 and S2 silica supports, are presented in Table 3 in terms of hourly CH_4 conversion (X_h, %), product selectivity (S_X, %), reaction rate ($\mu mol_{CH_4}\ s^{-1}\ g^{-1}$), space time yield ($STY_{HCHO}$, $g\,kg_{cat}^{-1}\,h^{-1}$), and specific Fe atomic rate (s^{-1}) of CH_4 conversion (Fe_{CH_4}) and HCHO formation (Fe_{HCHO}, $Fe_{CH_4} \times S_{HCHO}$).

Regardless of the preparation method and loading, Fe addition always results in a promoting effect of the intrinsic reactivity of any silica carrier [2,5–8,12,15], though it is fairly evident that the AP route generally permits a superior performance in MPO [9–12].

The bare S1 silica runs with an hourly CH_4 conversion of 2.7% and a S_{HCHO} equal to 66%, corresponding to a reaction rate of 2.8 $\mu mol\,g^{-1}\,s^{-1}$ and a STY_{HCHO} of 200 $g\,kg_{cat}^{-1}\,h^{-1}$. The S2 silica carrier, with both higher activity ($X_{CH_4,h}$, 3.8%) and S_{HCHO} (75%), ensures a STY_{HCHO} of 310 $g\,kg_{cat}^{-1}\,h^{-1}$. Normalised to the Fe content (Table 1),

Table 3
BR data of FeO_x/SiO_2 catalysts in MPO at 650 °C. Effect of the preparation method and Fe loading

Sample	$X_{CH_4,h}$ (%)	S_{HCHO} (%)	S_{CO} (%)	S_{CO_2} (%)	Rate ($\mu mol\,s^{-1}\,g^{-1}$)	STY_{HCHO} ($g\,kg_{cat}^{-1}\,h^{-1}$)	Fe_{CH_4} (s^{-1})	Fe_{HCHO} (s^{-1})
S2	3.8	75	16	6	3.8	310	1.06	0.75
S1	2.7	66	26	8	2.8	200	1.05	0.66
F[1000]S1-IW	8.6	55	28	17	8.8	525	0.50	0.27
F[1000]S2-IW	9.9	54	27	19	10.1	580	0.57	0.31
F[4300]S2-IW	7.8	47	22	31	10.4	405	0.14	0.06
F[3700]S2-AP	37.2	33	29	38	37.9	1350	0.57	0.19
F[1000]S1-AP	14.6	63	25	12	15.0	1020	0.84	0.53
F[3700]S1-AP	34.2	36	37	27	35.1	1360	0.53	0.19
F[3700]S2-AP[a]	4.6	55	23	22	47.3	2800	0.72	0.39
F[7300]S1-AP[a]	4.8	54	23	23	49.2	2870	0.38	0.20

[a] Catalyst testing at tenfold lower contact time (w_{cat}, 0.005 g).

however, the two silica samples feature analogous Fe_{CH_4} (1.05–1.06 s^{-1}) and Fe_{HCHO} (0.66–0.75 s^{-1}) values.

The addition of ca. 0.10 wt% Fe to the Si 4-5P carrier by IW (F[1000]S2-IW) implies a threefold rise in activity ($X_{CH_4,h}$, 9.9%) counterbalanced by a lowering in S_{HCHO} from 75 to 54%. Though there is a significant rise in STY_{HCHO} (580 $g\,kg_{cat}^{-1}\,h^{-1}$), the above figures account for a decrease in Fe_{CH_4} to 0.50 s^{-1} and, mostly, in the Fe_{HCHO} value (0.27 s^{-1}) with reference to the S2 carrier. The same amount of Fe (0.1 wt%) put on the F5 silica by IW (F[1000]S1-IW) attains a similar effect on activity ($X_{CH_4,h}$, 8.6%) and selectivity (S_{HCHO}, 55%), also in terms of Fe_{CH_4} and Fe_{HCHO} (Table 3). The addition of 0.43 wt% Fe to S2 silica, still by the IW route, has a strongly negative impact on the MPO functionality of the FeO_x/SiO_2 system, as the F[4300]S2-IW attains a X_h of 7.8%, resulting in a very low Fe_{CH_4} value (0.14 s^{-1}), coupled to a S_{HCHO} of 47%. These figures account for a STY_{HCHO} of only 405 $g\,kg_{cat}^{-1}\,h^{-1}$ and a Fe_{HCHO} value (0.06 s^{-1}) that is lower by about one order of magnitude than that of the F[1000]S2-IW sample.

The F[1000]S1-AP catalyst, bearing 0.1 wt% Fe on F5 silica by AP, is much more active (X_h, 14.6%) and selective (S_{HCHO}, 63%) than previous ones, featuring Fe_{CH_4} (0.84 s^{-1}) and Fe_{HCHO} (0.53 s^{-1}) values comparable to those of silica carriers and attaining a remarkable STY_{HCHO} of 1,020 $g\,kg_{cat}^{-1}\,h^{-1}$. A Fe content (3700 ppm) similar to that of the F[4300]S2-IW sample, added to S2 silica by AP (F[3700]S2-AP), yields an activity (X_h, 37.2%) fivefold larger than that of the counterpart IW sample, corresponding to an Fe_{CH_4} value of 0.57 s^{-1}. In spite of the "high" conversion level, this catalyst ensures a S_{HCHO} of 33%, accounting for a STY_{HCHO} of 1350 $g\,kg_{cat}^{-1}\,h^{-1}$ and a Fe_{HCHO} value of 0.19 s^{-1}. With Fe_{CH_4} (0.53 s^{-1}), Fe_{HCHO} (0.19 s^{-1}), and STY_{HCHO} (1360 $g\,kg_{cat}^{-1}\,h^{-1}$) values comparable to those of the homologous F[3700]S2-AP, activity data for the F[3700]S1-AP system confirm a slight, if any, effect of the silica carrier on activity, also at higher loading of the active phase.

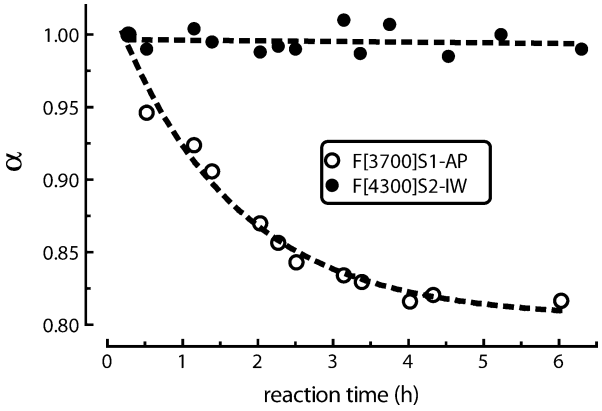

Fig. 4. MPO on FeO_x/SiO_2 catalysts (BR data at 650 °C). Effect of the preparation method on the relative activity (α) of the F[3700]S1-AP and F[4300]S2-IW catalysts during t.o.s.

The catalytic pattern of the most active F[3700]S2-AP and F[7300]S1-AP samples was also probed at a tenfold lower contact time (τ, 3.3×10^{-4} s) to avoid kinetic limitations imposed by high O_2 conversion [2,19–21] and compare their performance at conversion levels similar to those of less active catalysts (Table 3). Under such conditions the two catalysts feature similar X_h (4.6–4.8%) and S_{HCHO} (54–55%) values corresponding to STY_{HCHO} values equal to 2800–2900 $g\,kg_{cat}^{-1}\,h^{-1}$ [9–12,46].

At the least the influence of the preparation method on stability was evaluated by a comparison of the relative activity α (e.g., the ratio between activity at time t, $X_{h,t}$, and time zero, $X_{h,0}$) of AP and IW catalysts during t.o.s. Depending on the preparation method, a different stability pattern is recorded, as shown in Fig. 4, comparing representative data for the F[3700]S1-AP and F[4300]S2-IW samples. That is, while the latter catalyst keeps both activity and selectivity substantially stable throughout the test, the former undergoes a ca. 20% activity loss with a concomitant decrease in S_{HCHO} (from 36 to 30%) after 6 h of t.o.s. Notably, this resulted a common pattern for all AP catalysts and IW samples with Fe loading less than 0.4 wt%.

Table 4
CF activity data of FeO_x/SiO_2 catalysts in MPO in the T range 400–750 °C

Catalyst	$T_{1\%}$ (°C)	S_{HCHO} (%)	$T_{2\%}$ (°C)	S_{HCHO} (%)	$T_{5\%}$ (°C)	S_{HCHO} (%)	E_{app} (kJ/mol)
S2	620	48	650	44	710	35	142
F[1000]S2-IW	520	24	565	22	630	18	88
F[4300]S2-IW	530	11	575	8	630	7	101
F[3700]S2-AP	455	9	500	8	570	8	85
F[1000]S1-AP	500	28	545	24	620	20	82
F[3700]S1-AP	460	12	495	11	565	10	83
F[5900]S1-AP	466	11	505	10	570	9	84
F[1000]S1-AP[a]	525	54	570	49	–	–	110
F[3700]S2-AP[a]	490	20	530	19	–	–	110

[a] CH_4/O_2 ratio, 40.

3.2.2. CF activity data

Integral activity data in the range of 400–750 °C (τ, 6.6×10^{-2} s) are compared in Table 4 in terms of temperature of 1% ($T_{1\%}$), 2% ($T_{2\%}$), and 5% ($T_{5\%}$) CH_4 conversion, HCHO selectivity (S_{HCHO}), and apparent activation energy values (E_{app}, kJ/mol), calculated in the CH_4 conversion range of 1–10%.

The S2 carrier attains 1% CH_4 conversion at 620 °C with a S_{HCHO} equal to 48%, prompting 2 and 5% conversion levels at 650 °C (S_{HCHO}, 43%) and 710 °C (S_{HCHO}, 35%), respectively. These mirror an apparent activation energy value of 142 kJ/mol [2,20], resulting the highest in the series (Table 4).

In agreement with BR data, the higher activity of AP catalysts emerges from a shift of all of the conversion levels to lower temperature (Table 3), consistently with a decrease in the activation energy (E_{app}, 83–101 kJ/mol). The F[1000]S1-AP and F[1000]S2-IW samples feature a similar catalytic pattern, denoted by the attainment of 1% CH_4 conversion ($T_{1\%}$) and an analogous S_{HCHO} (25–27%) at 500–520 °C. Mirroring a similar drop in the E_{app} (82–88 kJ/mol), both $T_{2\%}$ and $T_{5\%}$ are also shifted to lower temperature by ca. 100 °C, and the S_{HCHO} decreases to 20–22 and 18–20%, respectively. The addition of higher Fe loadings (0.37–0.59 wt%) to F5 silica by AP, shifts the conversion levels further to the same lower temperature (450–460 °C), and, though the S_{HCHO} decreases to 9–12%, no changes in the E_{app} (83–85 kJ/mol) are noticed. Meanwhile, CF data for the F[3700]S2-AP sample confirm the minor influence of the silica carrier on the MPO activity of FeO_x/SiO_2 catalysts (Table 4). In contrast, the F[4300]S2-IW sample displays the highest $T_{x\%}$ values, along with the lowest S_{HCHO} values in the series and, consequently, the resulting E_{app} (101 kJ/mol) is between the highest (142 kJ/mol) and the lowest (82–88 kJ/mol) values found for S2 and AP catalysts, respectively.

The performance of AP systems has been also probed under oxygen-lean conditions with a feed of a 90% CH_4/2.3% O_2/7.7% He reaction mixture and a constant contact time (τ, 6.6×10^{-2} s). In spite of the high CH_4/O_2 ratio (≈ 40) hindering the reaction kinetics [2,19–21], the F[1000]S1-AP sample attains 1% (525 °C) and 2% (570 °C) conversion levels at a temperature slightly higher than at standard conditions (CH_4/O_2, 2), whereas a more than twofold rise in S_{HCHO} (54 and 49%) accounts for STY_{HCHO} values of 360 and 650 $g\,kg_{cat}^{-1}\,h^{-1}$ at 525 and 570 °C, respectively. A larger shift of both $T_{1\%}$ and $T_{2\%}$ to higher temperature (Table 4) does not affect a similar increase in S_{HCHO} on the F[3700]S1-AP sample (Table 4).

3.3. Characterisation of the "treated" and "used" catalysts

3.3.1. TPR of catalysts pretreated (650 °C) with CH_4 and CH_4/O_2 reaction mixture flow

The TPR profiles of F[3700]S1-AP (A) and F[4300]S2-IW (B) catalysts, pretreated for 5 min at 650 °C under flowing CH_4 (top), are compared with the corresponding profiles of the calcined samples (bottom) in Fig. 5A. Regardless of the preparation method and Fe loading, the treatment of FeO_x/SiO_2 catalysts at 650 °C with methane causes a marked decrease in the TPR signal in the T range of 350–650 °C, evidently diagnostic of an extensive reduction of Fe^{3+} ions to Fe^{2+} by the substrate. This reflects significant changes in the respective reduction profile, no longer showing the typical features of the calcined systems.

Furthermore, the reduction patterns of the "used" F[3700]S1-AP and F[4300]S2-IW catalysts have been compared with the relative spectra of "fresh" samples in Fig. 5B. The TPR profile of the "used" F[3700]S1-AP catalyst shows marked changes in the reduction kinetics, evidently diagnostic of a deep *reconstructuring* of the active phase, whereas only a slight decrease in the rate of H_2 consumption on the rising side of the main TPR peak is noticed for the F[4300]S2-IW system. As a consequence, the TPR spectra for the "used" systems look similar to each other, reproducing, in turn, almost unchanged the main features of the "fresh" F[4300]S2-IW sample.

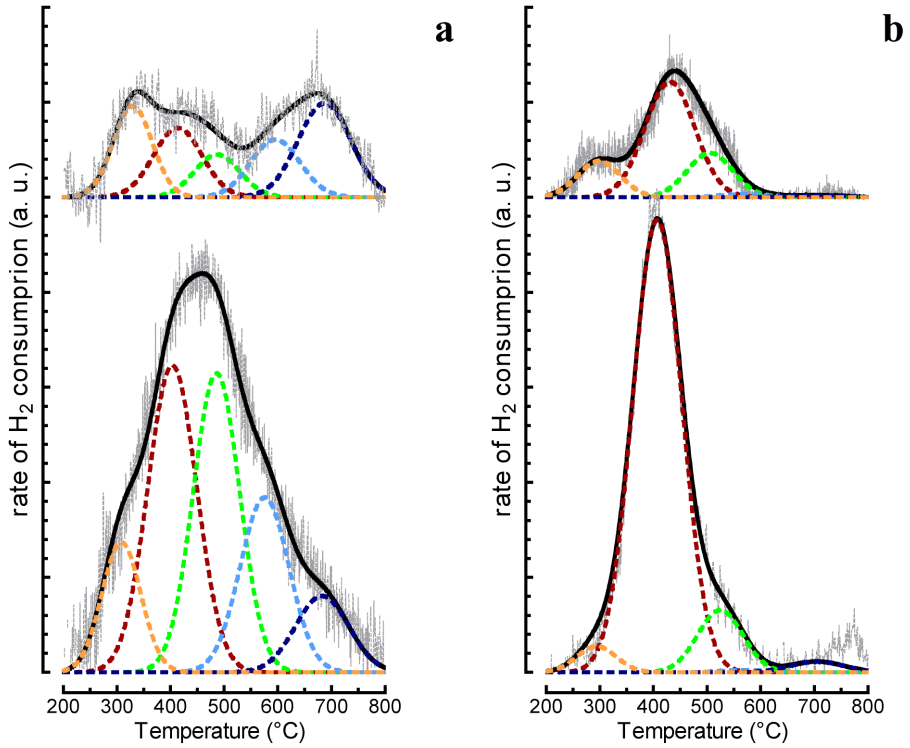

(A)

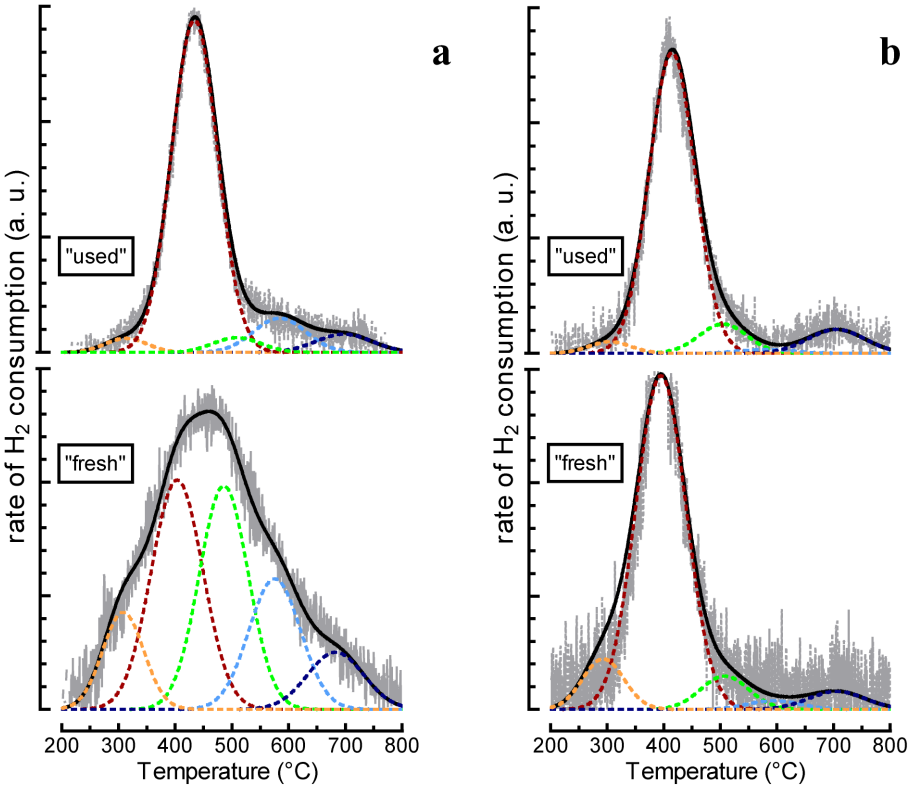

(B)

Fig. 5. (A) Comparison of TPR spectra of the F[3700]S1-AP (a) and F[4300]S2-IW (b) catalysts, pre-treated (5 min) at 650 °C with a 10%CH_4/He flow (top), with those of "fresh" samples (bottom). (B) Comparison of TPR spectra of "fresh" (bottom) and "used" (top) F[3700]S1-AP (a) and F[4300]S2-IW (b) catalysts.

4. Discussion

4.1. Structure of low-loaded FeO_x/SiO_2 catalysts

Although a relatively poor concentration and reactivity of the hydroxyl population in comparison with other oxide supports (e.g., alumina, titania, zirconia, etc.), yet, at a molecular scale the silica surface exhibits some chemical affinity for supported metal atoms and/or ions [47,48], along with some reactivity towards gas phases [2,3,13,49]. "Molecular" dispersion, then, entails a hard reducibility of supported species, owing to the *electron-withdrawal* effect exerted by the oxygen-bridged bonds, the extent of which depends upon the structure of guest "hollow" sites of the silica surface [22,30,47,48,50,51]. On the basis of Mössbauer, IR spectroscopy, and volumetric/gravimetric adsorptions, then, Dumesic et al. argued that two states of Fe^{2+} exist in a reduced 1 wt% Fe/SiO_2 catalyst: *Fe^{2+} strongly interacting with the support* and *Fe^{2+} in small particles of iron oxide* [22]. They stressed that the former should be present as *thin "rafts"* on the support, holding mostly Fe^{2+} in a *low coordination*, whereas *high-coordinated* Fe^{2+} are present at the surface of iron oxide particles [22]. A strong interaction with silica hinders the reduction of both to the metallic state [22], involving also Si^{4+}/Fe^{3+} lattice substitution(s) in tetrahedral sites of the magnetite structure [50].

In fact, the stabilisation of *Fe_2O_3 particles*, *oxide nanoclusters*, *isolated iron ions*, and *oxygen-bridged iron ions* does not depend upon the oxide support, being a function of preparation method [22–28,30], loading [22–25,30,51], and thermal treatments [22–30]. In this context, the chemistry of iron and oxide support in aqueous solution plays an essential role. That is, avoiding an uncontrolled precipitation of the iron hydroxide (i.e., pK_s $Fe(OH)_3 \cong 38$ vs. pK_s $Fe(OH)_2 \cong 12$) and exploiting the "selective" interaction of negatively charged silanolate groups with Fe^{2+} cations at $pH > pH_{ZPC}$, the AP route favours an effective dispersion of Fe^{2+} ions all over the SiO_2 surface [2,9–12] according to the DR UV–Vis absorption pattern, monitoring the prevailing contribution of "isolated" and "oligomeric" Fe^{III}–O_x species in the F[xxxx]S1-AP series (Fig. 1B). However, the shift of the absorption maximum, as the loading increases, signals a growing degree of aggregation of the surface FeO_x species, forming *2-d patches* over the silica surface [22,27–29]. In contrast, despite a SSL comparable with that of the F[5900]S1-AP sample (Table 1), an absorption fairly shifted to lower wavenumbers and the intense absorption in the 20,000–10,000 cm^{-1} range (Fig. 1A, spectrum c) denote that Fe_2O_3 particles are largely present on the F[4300]S2-IW system, as a consequence of the lack of any effective interaction between silica and Fe^{3+} ions throughout IW impregnation [8–12].

Thus, indicating a close relationship between dispersion and redox properties of the active phase, the marked shift of the main TPR maximum from 570–580 to ca. 400 °C, going from bare silica to F[4300]S2-IW, F[3700]S2-AP and F[7300]S1-AP samples (Fig. 3), then monitors the reduction of Fe^{3+} ions belonging to various surface structures. And so a systematic comparison of UV–vis and TPR features indicates that the reduction of "isolated" Fe moieties, characterised by the strongest interaction with the support, falls in the temperature window of 550–750 °C, where the contribution of several components is evident from TPR profiles of silica carriers (Fig. 3, profiles a). Such species drive the redox cycle with the substrate [2,8,12,16,19,20,36], being then responsible for the effective catalytic pattern of "precipitated" silica [13,36,49]. At the opposite tendency, the spectroscopic results for the F[4300]S2-IW sample signal an almost quantitative contribution of hematite nanoparticles, the reduction of which matches a symmetric peak centred at ca. 400 °C (Fig. 3C, profile b). Therefore, a weaker interaction with the silica matrix of Fe^{3+} ions therein prompts an easier reducibility with a rising degree of aggregation of the active phase [6,7,9,11,22–28]. Mirroring a variable contribution of various surface structures, then, the TPR profiles of the FeO_x/SiO_2 system bear quantitative information on the abundance of the various surface structures that is unavailable from spectroscopic measurements. For instance, while the TPR pattern of the F[4300]S2-IW sample (Fig. 3C, profile b) matches satisfactorily with spectroscopic findings, Mössbauer data for the F[7300]S1-AP sample indicate that a significant fraction (ca. 50%) of the active phase is in the form of Fe_2O_3 nanoparticles, the presence of which is barely visible, if at all, from the relative UV–vis absorption pattern (Fig. 1B, profile d). Since deconvolution of TPR spectra previously made it possible to highlight the structure of supported V_2O_5 [35,36] and MoO_3 [34,36] catalysts, an analogous approach was adopted in the attempt to assess the *speciation* of the active phase in the FeO_x/SiO_2 system.

4.2. Speciation and dispersion of the active phase

According to previous EPR [8] and FTIR data for adsorbed NO [46,52], spectroscopic findings suggest that the TPR pattern of FeO_x/SiO_2 catalysts monitors the cumulative reduction of the following surface structures:

(i) "Isolated" Fe^{III} ions located on different *hollow* sites of the carrier, with a different degree of surface coordination [6–11,46,52];
(ii) 2-d aggregated Fe^{III} species, forming thin "rafts/patches" on the silica surface [22,46,52];
(iii) 3-d Fe_2O_3 particles, the reduction of which depends mostly on crystal size [6–11,22,46,52].

Interaction strength, with matrix, spatial structure, and coordination environment, controls the reducibility of Fe^{III} ions in the above surface species [11,46,51,52]. Then the adopted modelling procedure implies that, at a given temperature, the rate of catalyst reduction results from the cumulative contribution of the various surface species, characterised by a *normal* distribution of the activation energy

Table 5
Fitting parameters of TPR spectra of "fresh", "pre-treated" and "used" FeO_x/SiO_2 catalysts

Sample	Surface species									
	3-d Fe_2O_3 clusters				2-d FeO_x patches		Isolated Fe^{III} species			
	M_0/fwhm$_0$ (°C)	A_0 (%)	M_1/fwhm$_1$ (°C)	A_1 (%)	M_2/fwhm$_2$ (°C)	A_2 (%)	M_3/fwhm$_3$ (°C)	A_3 (%)	M_4/fwhm$_4$ (°C)	A_4 (%)
"Fresh" catalysts										
S1	280/85	2.7	420/107	11.0	529/99	29.4	614/108	27.0	724/118	29.8
S2	300/85	1.6	407/104	7.8	521/99	20.8	619/107	34.0	726/117	35.6
F[1000]S1-AP	315/85	4.0	393/108	17.7	501/99	31.3	607/108	23.1	716/117	23.9
F[1300]S1-AP	315/85	2.7	399/108	23.2	493/99	28.9	577/107	21.5	696/117	23.7
F[3700]S1-AP	316/85	6.8	400/108	29.0	485/99	31.8	586/108	18.5	700/117	13.9
F[5900]S1-AP	308/85	10.9	403/107	32.3	486/99	30.1	575/107	18.0	683/117	8.7
F[7300]S1-AP	312/85	10.8	407/107	43.9	496/99	20.4	582/108	12.9	696/117	12.0
F[3700]S1-AP	316/85	6.8	400/108	29.0	485/99	31.8	586/108	18.5	700/117	13.9
F[3700]S2-AP	313/85	8.7	396/107	40.6	479/99	25.0	572/108	14.3	691/117	11.3
F[4200]S1-IW	301/85	7.5	409/107	39.8	505/99	20.3	589/108	21.4	685/117	11.0
F[4300]S2-IW	296/85	6.7	397/107	79.3	504/99	5.5	595/108	2.4	705/117	6.2
F[1000]S1-IW	294/85	5.0	423/107	23.0	526/99	36.9	594/108	9.5	675/117	25.5
F[1000]S2-IW	299/85	2.6	396/107	25.2	494/98	39.3	581/108	18.5	678/117	15.2
"Pre-treated" catalysts										
F[3700]S1-AP	282/85	10.4	411/107	18.5	509/99	24.0	600/108	22.3	690/117	24.7
F[4300]S2-IW	296/88	16.0	427/108	60.1	506/99	1.0	578/108	1.7	704/117	1.3
"Used" catalysts										
F[3700]S1-AP	305/85	4.4	423/100	67.4	491/99	13.7	576/107	8.3	685/117	6.1
F[4300]S2-IW	304/85	4.7	412/100	81.7	505/99	6.1	582/108	1.0	705/117	6.5

for reduction [34–36,52]. In fact, by a preliminary iterative procedure it was found that all of the TPR profiles can be described by a linear combination of five Gaussian peaks, with the same centre position (M, °C) and full width at half-maximum (fwhm, °C), and only a variable intensity (A, %) [11,34–36,52]. Representative results for TPR spectra modelling are shown in Fig. 6, displaying the deconvoluted TPR spectra of differently loaded S1-supported AP systems (see Fig. 3A). The parameters of the Gaussian components used for the deconvolution of all TPR spectra are summarised in Table 5. Although a scale factor of ca. 50 in the iron concentration (Table 1), implying remarkable differences in the sample loading (25–500 mg) throughout TPR measurements, likely explains some variations in M (±20 °C) and fwhm (±8 °C) values (Table 5), the fact that the same component keeps an unchanged centre position and fwhm can be taken as a reliable index of the same nature (and interaction path) of the various Fe^{3+} species with silica regardless of preparation route, Fe loading, and silica carrier [34–36]. Then the following attribution can be inferred.

The first component (peak 1) centred at ca. 400 °C monitors the reduction of 3-d "aggregates," mostly in the form of *Fe_2O_3 nanoclusters*.

The second component (peak 2), with the maximum at ca. 500 °C, would be associated with the reduction of 2-d *$(–Fe–O–Fe–)_n$ patches* (i.e., thin "rafts") linked to the silica surface by a network of "Fe–O–Si" bonds and, thus, resulting in less reducibility than that of oxide *nanoclusters*.

The third (peak 3) and fourth (peak 4) components, centred at ca. 600 and 700 °C, respectively, match with a poor reducibility of isolated Fe^{3+} ions in a T_d-like coordination [6–9,11,46,51,52]. Their reducibility depends upon the number of "Fe–O–Si" linkages in the first coordinative shell and, thus, on location across different *hollow* sites of the silica surface [47,48]. Indeed, previous FTIR data for adsorbed NO indicated that only mono-nitrosyls form at an Fe loading of ca. 1000 ppm (F[1000]S1-AP), whereas at higher loadings (F[3700]S1-AP) both mono- and tri-nitrosyl adducts form on Fe^{II} ions belonging to mono/oligomeric moieties [46]. These results have been rationalised by considering that a number of structures exist on the surface of the supports [47,48], depending on the location in "smaller" or "large" $(SiO_2)_n$ rings. The fewer oxygen atoms in the former, because of their propinquity, tend to strongly stabilise "entrapped" Fe^{3+} ions. As a consequence, these structures are the first to "graft" incoming Fe ions at lower loading, by ensuring a higher shielding. "Large" rings accommodate transition-metal ions only at higher loading, implying an enhanced coordinative unsaturation. Thus isolated Fe^{3+} ions, bearing multiple surface oxygen bridged bonds and located in smaller hollow sites, are the most resistant to reduction and can therefore be associated with the fourth component. A higher degree of coordinative unsaturation of isolated Fe^{III} ions located in larger hollow sites implies an easier reducibility and can be then associated with the third component.

Perhaps, such an assignment explains the fact that Dumesic et al. could not detect isolated Fe^{2+} ions in a 1% Fe/SiO_2 catalyst reduced at 500 °C, but rather Fe^{2+} ions of low coordination in some *2-d* "thin rafts" along with high-coordination Fe^{2+} ions of 3-d Fe_2O_3 clusters [22].

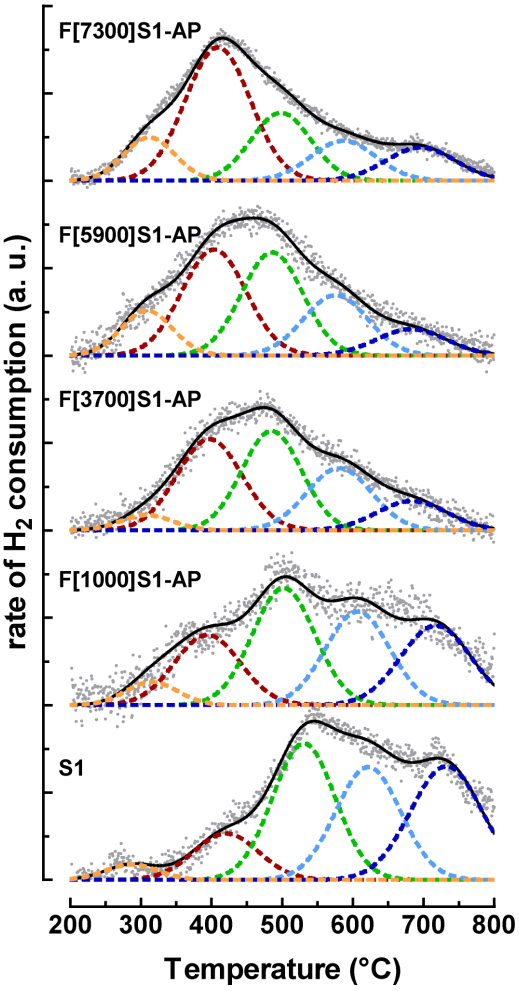

Fig. 6. Modelling of TPR spectra of F[xxxx]S1-AP catalysts (see Fig. 3A).

Concerning the zeroth component, its fate with loading and preparation method makes the relative assignation less straightforward, and hence requiring specific reasoning. That is, it is almost absent on systems with a very low ($\leqslant$ 1000 ppm) Fe loading, where the presence of Fe_2O_3 aggregates is also rather poor (Table 5). Its relative intensity rises abruptly to ca. 22% of that of the Fe_2O_3 component, remaining almost unchanged ($\approx$ 25%) up to the F[7300]S1-AP catalyst (Table 5). Moreover, at a comparable Fe loading, the intensity ratio of the 0th and first components on IW systems is quite lower than on counterpart AP systems, whereas for the same preparation route, F5 supported systems feature a higher value of this ratio (Table 5). Finally, the F[4300]S2-IW features the lowest value (8%) of the above ratio. These findings suggest that the 0th peak is somewhat related to the *dispersion* of oxide aggregates, thus belonging to reduction of Fe^{3+} ions at the surface of oxide nanoparticles, though it could also refer to some intermediate (e.g., Fe_3O_4) reduction step.

By this account, the speciation of the active phase in both F[xxxx]Sy-AP and F[xxxx]Sy-IW catalysts can be generally related to the SSL, as shown in Fig. 7A, comparing the relative percentage of Fe^{III} ions in the various surface structures. As expected, the concentration of isolated moieties decreases monotonically with SSL, whereas that of 3-d oxide particles rises much more steadily with an exponential-like trend (Fig. 7A). On the other hand, the featureless trend of 2-d patches matches is consistent with the fact that these are "borderline" structures, easily evolving into 3-d oxide clusters. However, the different trends of AP (solid lines) and IW (dotted lines) systems indicate that, in addition to the SSL, the preparation route is crucial for the stabilisation of the various surface structures of the FeO_x/SiO_2 system. Indeed, with respect to Mo [34,36] and V [35,36], Fe^{III} ions feature a much lower chemical affinity for the silica surface, since an amount of Fe_2O_3 clusters comparable to that found on bare silicas (ca. 15%) was detected at much larger SSL on MoO_3/SiO_2 [34,36] and V_2O_5/SiO_2 [35,36] systems. Furthermore, a ca. 80% concentration of oxide particles, like that found on the F[4300]S2-IW sample (ca. 0.1 Fe_{at} nm^{-2}), occurs on a 7% MoO_3/SiO_2 bearing a 50-fold larger SSL [34,36]. This different behaviour indicates that a weaker interaction of Fe^{III} ions with silonalol groups is the driving force for the poor dispersion of the active phase in IW systems, whereas, favouring a stronger metal-support interaction, the AP route hinders the mobility of Fe ions and formation of 3-d oxide clusters also on the "highly loaded" F[7300]S1-AP sample (SSL $\approx$ 0.14 Fe_{at} nm^{-2}).

The assumptions of deconvolution analysis then make it possible to define the dispersion, D, of the active phase as the ratio between the concentration of "exposed" Fe atoms in the various structures (i.e., $A_0 + A_2 + A_3 + A_4$) and the total number of Fe atoms reduced up to 750 °C (i.e., $A_0 + A_1 + A_2 + A_3 + A_4$)

$$D = \frac{N_{\mathrm{Fe_{surface}}}}{N_{\mathrm{Fe_{total}}}} = \frac{\sum(A_0 + A_2 + A_3 + A_4)}{\sum(A_0 + A_1 + A_2 + A_3 + A_4)}.$$

Dispersion of AP and IW catalysts as a function of the respective SSL is shown in Fig. 7B. It is evident that whereas the AP route ensures a rather good dispersion (0.85–0.55) of the active phase, decreasing regularly with SSL to the value of ca. 0.15 Fe_{at} nm^{-2}, the IW implies an *unpredictable* extent of aggregation of the active phase, which is more evident for SSL exceeding the value of 0.05 Fe_{at} nm^{-2} (Table 1) [8–13]. The influence of the silica carrier is then mostly linked to the specific surface area and relative SSL [34–36].

4.3. Surface structures and catalytic activity

The thermodynamic driving force for consecutive oxidation(s) of organic molecules into more stable carbon oxide(s) entails the running of selective oxidations under a kinetic regime. In terms of catalyst features, moreover, selective oxidations demand oxide systems bearing specific ensemble(s) of active sites with a strength of the metal–oxygen bond timely tuned on the reactivity of the substrate [2,6,7,16,53,54]. In particular, "isolated" Fe^{3+} ions supported on silica carriers join an enhanced functionality for

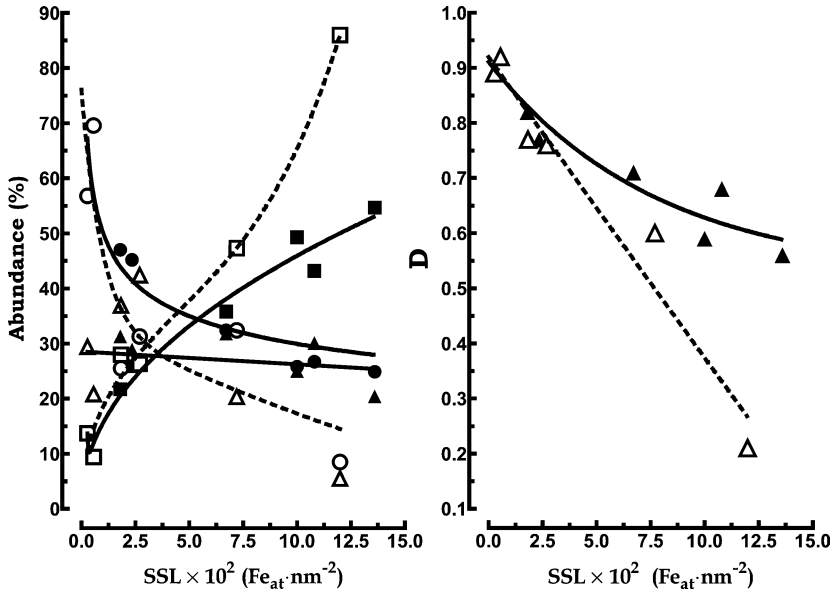

Fig. 7. (A) Influence of the Fe surface loading (SSL) on the relative concentration of the various surface species (○, ● isolated species; △, ▲ 2-d FeO_x patches; □, ■ 3-d oxide particles) in AP (solid symbols and lines) and IW (open symbols–dotted lines) systems. (B) Influence of the SSL on dispersion of the active phase (D) of the FeO_x/SiO_2 system: (●) AP and (○) IW catalysts.

CH_4 activation with a remarkable selectivity for oxygenated products [6–12], resulting in a MPO performance superior to that of any other system [6,12,13]. Ab initio quantum-chemical calculations suggest that this outstanding catalytic behaviour arises from an intrinsic efficiency of the FeO^+ complex in activating the CH_4 molecule, driving its primary oxy-functionalisation to CH_3OH [17,18], whereas 3-d Fe_2O_3 structures depress the catalytic functionality of the title system because of a poor dispersion and the enhanced reducibility of the surface Fe^{3+} centres [7–11,46,52]. On the whole these findings match with the "*site isolation*" requirement, well known in the field of selective oxidation reactions [1,12,16,53–56], postulating that a desired reaction path proceeds over an ensemble of active sites containing the minimum number of centres for substrate activation and functionalisation [1,2,12,53–56], whereas a high availability and mobility of nucleophylic lattice $O^=$ species, typical of bulk oxide clusters [6,8,53,54], is detrimental for intermediate product lifetime. Although BR and CF catalytic data (Tables 3 and 4) confirm the superior functionality of AP catalysts arising from a higher dispersion of the active phase on silica carriers (Fig. 7B), previous kinetic-mechanistic findings indicated a second-order dependence of CH_4 activation rate on the concentration of active sites [21]. The plot of Fe_{CH_4} values vs. *D* of the various catalysts, shown in Fig. 8, really provides a satisfactory experimental support for that theoretical relationship, confirming the superior dependence of substrate activation on site concentration [2,16,19–21]. Moreover, the product selectivity is even more sensitive to the degree of aggregation of the active phase, since the different reducibilities of the various surface structures determine the type and concentration of oxygen species (O_2^-, O_2^{2-}, O^-, etc.) featuring an *electrophilic* or *nucleophilic* character and, then, a different reactivity towards CH_4 and/or intermediates (CH_3OH/HCHO) [1,12,16,53,54]. Thus an easy reducibility would permit the prevailing formation of O^{2-} ions at the surface of oxide nanoparticles, prompting the conversion of HCHO into CO_x by a nucleophilic attack on the C atom, whereas the poor *electron availability* of dispersed species leads mostly to the formation of electrophilic oxygen species that are more active towards the unpolarised C–H bond of the methane molecule. This indicates that an effective MPO functionality is enabled by dispersion values higher than 0.5 (Fig. 8).

Deeper insight into the reactivity of various surface species can be achieved from TPR data for CH_4-pretreated catalysts (Fig. 5A). Notably, despite the relevant changes with respect to those of the calcined systems, these reduction patterns result still from the linear combination of the (same) five Gaussian components used for the deconvolution of the TPR spectra of the "fresh" systems (Fig. 6), according to the fitting parameter values listed in Table 5. The relative intensities of the various components in "fresh" and "CH_4-pretreated" systems, shown in Fig. 9A, points to a marked decrease in the *peak 1* and, to a lower extent, in *peaks 2* and *3*, previously assigned to the reduction of "*3-d Fe_2O_3 clusters*" (peak 1), "*2-d FeO_x polymeric patches*" (peak 2), and "*low-coordination isolated*" species (peak 3), respectively. Despite the considerable (> 70%) reduction of 3-d Fe_2O_3 species, the decrease in the component (*peak 0*) relative to Fe^{3+} ions at the surface of oxide particles is less pronounced (20–40%), whereas the intensity of the *peak 4* related to the reduction of "strongly-interacting" isolated species is almost unchanged. A marked decrease in the peak area relative to oxide clusters (peak 1) and, to a lesser extent, in 2-d FeO_x patches (peak 2) and low-coordinated

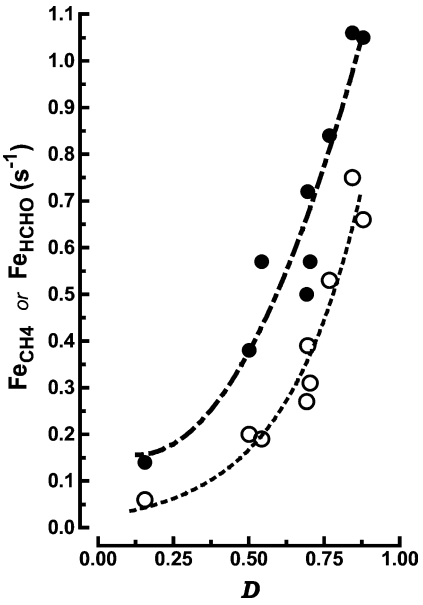

Fig. 8. Relationship between the Fe atom specific rate (s^{-1}) of CH_4 conversion (Fe_{CH_4}) and HCHO formation (Fe_{HCHO}) and oxide dispersion (D), evaluated from modelling of TPR spectra.

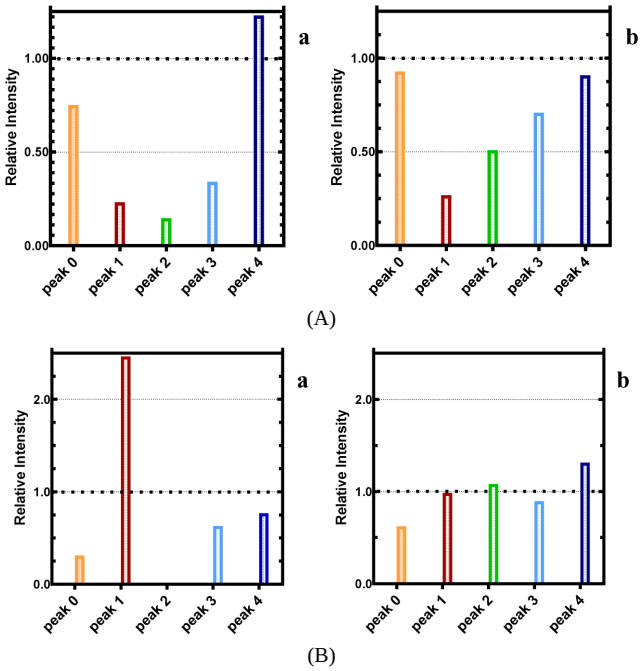

Fig. 9. (A) Relative intensity of the (five) Gaussian components adopted for deconvolution of TPR spectra of the F[3700]S1-AP (a) and F[4300]S2-IW (b) catalysts pre-treated (5 min) at 650 °C in CH_4 flow. (B) Relative intensity of the (five) Gaussian components of the "used" F[3700]S1-AP (a) and F[4300]S2-IW (b) catalysts.

Fe^{3+} ions (peak 3) is diagnostic of an increasing strength of the "Fe–O" bond, rendering oxygen atoms kinetically less available for methane (over)oxidation. The lowest reducibility of high-coordinated Fe^{3+} ions (peak 4) hinders any interaction with the substrate at 650 °C. Therefore, taking into account that the reactivity towards CH_4 parallels the reducibility of the various surface structures, a decrease of the 0th component comparable to or even stronger than that of oxide particles (peak 1) should be expected. A plausible explanation for the slight changes in the intensity of this component (Fig. 9A) lies in a high diffusion rate of O^{2-} ions across the lattice of Fe_2O_3 nanoparticles, stabilising mostly Fe^{3+} ions at the surface. This, in addition to accounting for the low activity and selectivity of poorly dispersed systems (Tables 2 and 3), also explains the "oxygen-release" phenomenon observed on FeO_x/SiO_2 catalysts characterised by high concentrations of 3-d oxide species during RTOC measurements [8,10]. Overall, these findings suggest that 2-d FeO_x patches, featuring an intermediate strength of the oxygen bond and a limited availability of oxygen ions, ensure the best MPO activity–selectivity pattern. In fact, the slight shift of 1 and 2% conversion levels recorded on the F[1000]S1-AP sample under oxygen-lean conditions (Table 4) signals an easier occurrence of the redox reaction cycle on such a system featuring a catalytic pattern dominated by 2-d FeO_x patches. The variable extent of the energetic barrier further supports this evidence, as E_{app} is the highest (142 kJ/mol) on the silica, which contains only 200 ppm Fe, mostly as isolated ions, and the lowest (80–85 kJ/mol) on the AP FeO_x/SiO_2 catalysts, which feature a catalytic pattern dominated by higher concentrations of 2-d FeO_x patches. The higher degree of nuclearity of such species, likely enabling a more effective transfer of electrons and reaction intermediates, could explain the decrease in the energetic barrier with respect to bare silica. In contrast, and inconsistent with the overwhelming concentration of *easily reducible* oxide (nano)particles, the intermediate E_{app} value (101 kJ/mol) of the F[4300]S2-IW sample likely stems from the intrinsic difficulty generating electrophilic oxygen species from easily reducible Fe_2O_3 aggregates (required by CH_4 activation [12,16,53,54]), owing to a high electron availability in the crystal lattice [6–12]. The fact that in the pretreated sample the relative concentration of oxidised Fe^{3+} ions at the surface of oxide species is much larger than in the bulk strengthens the above hypothesis. Therefore, such findings prove that different electronic features of the Fe–O bond parallel the structure of the various surface FeO_x species, prompting, as a consequence, different oxygen activation paths according to the scheme drawn in Fig. 10. Deconvolution analysis of TPR spectra for the "used" catalysts (Fig. 5B) indicates that the changes in the TPR pattern of the "used" F[3700]S1-AP sample stem mostly from the quantitative transformation of *2-d FeO_x patches* (peak 2) and, to a small extent, of *isolated moieties* (peaks 3 and 4) into *3-d Fe_2O_3 clusters* (peak 1), as shown in Fig. 9B. On the other hand, the changes in the structure of the F[4300]S2-IW sample, which is characterised by an overwhelming concentration (> 85%) of aggregated 3-d oxide particles, appear to be negligible. This result is a direct consequence of the surface-assisted redox reaction cycle, involving a cyclic sequence of rupture and formation of metal–oxygen bonds as a result of the alternate activation of substrate and oxy-

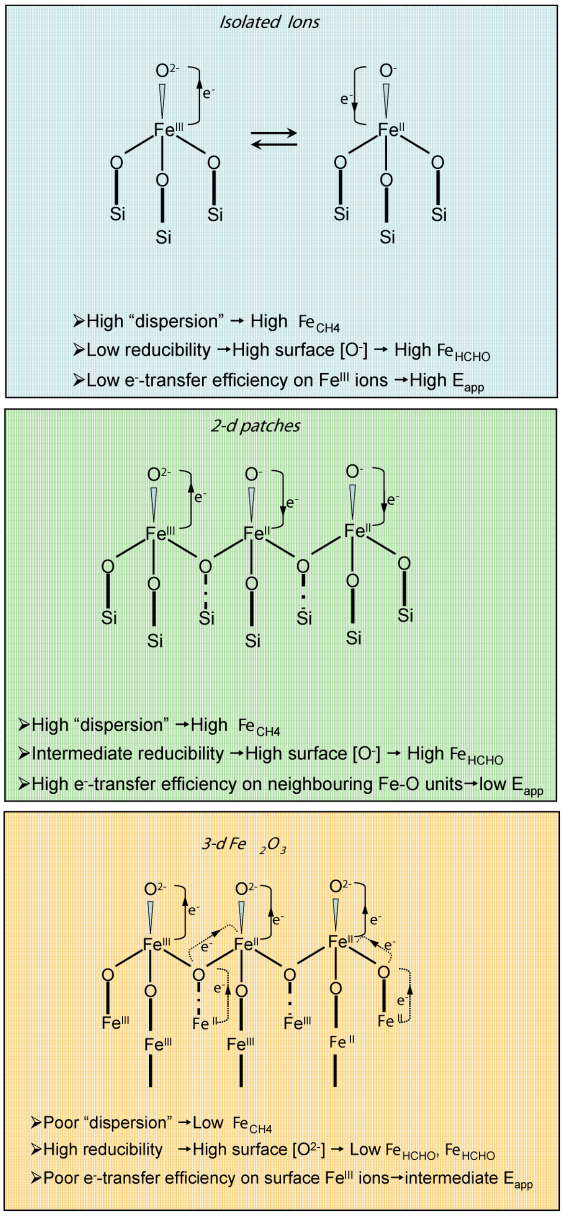

Fig. 10. Surface structures of FeO_x/SiO_2 catalysts and relative reactivity pattern.

gen, respectively [2–6,12,16–21,53,54]. As for the rupture of Fe–O–Si(Fe) bridged bonds, the redox cycle prompts the "mobility" of Fe^{3+} ions and the consequent sintering, which affects the stability of AP systems (Fig. 4) in a way analogous to the effect on the stability of well-dispersed Fe-ZSM5 systems in the SCR of NO_x, causing the "extraction" of Fe^{3+} ions from the zeolite framework [25,57].

5. Conclusions

The *adsorption/precipitation* method is much more effective than *incipient wetness* in promoting the dispersion of iron across silica carriers.

The *speciation* of the active phase determines the reduction pattern of the FeO_x/SiO_2 system.

"*Isolated species*," *2-d* $(FeO_x)_n$ *patches* and *3-d* Fe_2O_3 *clusters*, coexist on the surface of silica carriers and FeO_x/SiO_2 catalysts; their relative abundance depends on the preparation method and surface loading.

The *adsorption/precipitation* method strongly enhances the MPO performance of FeO_x/SiO_2 catalysts by improving the dispersion of the active phase.

The redox reaction cycle yields sintering phenomena of the active phase, causing a progressive deactivation of FeO_x/SiO_2 catalysts.

Acknowledgments

This work was partially realised in the framework of a research contract between "SÜD CHEMIE AG" (München, Germany) and "Dipartimento di Chimica Industriale e Ingegneria dei Materiali," Unime (Messina, Italy), during the period of August 2000 to July 2002.

References

[1] S. Albonetti, F. Cavani, F. Trifirò, Catal. Rev.-Sci. Eng. 38 (4) (1996) 413.
[2] F. Arena, A. Parmaliana, Acc. Chem. Res. 36 (12) (2003) 687.
[3] M.J. Brown, N.D. Parkyns, Catal. Today 8 (1991) 305.
[4] K. Otsuka, Y. Wang, Appl. Catal. A 222 (2001) 145.
[5] K. Tabata, Y. Teng, T. Takemoto, E. Suzuki, M.A. Bañares, M.A. Peña, J.L.G. Fierro, Catal. Rev.-Sci. Eng. 44 (1) (2002) 1.
[6] T. Kobayashi, K. Nakagawa, K. Tabata, M. Haruta, J. Chem. Soc., Chem. Comm. (1994) 1609.
[7] T. Kobayashi, Catal. Today 71 (2001) 69.
[8] A. Parmaliana, F. Arena, F. Frusteri, A. Martinez-Arias, M. Lopez-Granados, J.L.G. Fierro, Appl. Catal. A 202 (2002) 163.
[9] F. Arena, F. Frusteri, T. Torre, A. Venuto, A. Mezzapica, A. Parmaliana, Catal. Lett. 80 (2002) 69.
[10] A. Parmaliana, F. Arena, F. Frusteri, A. Mezzapica, Fe-Doped Silica Catalysts for the Partial Oxidation of Methane to Formaldehyde with Oxygen, German Patent No. GEM 17 (2000) (in the name of SÜD CHEMIE AG).
[11] F. Arena, F. Frusteri, L. Spadaro, A. Venuto, A. Parmaliana, Stud. Surf. Sci. Catal. 143 (2002) 1097.
[12] F. Arena, A. Parmaliana, Rec. Res. Dev. Catal. 2 (2003) 251.
[13] F. Arena, F. Frusteri, A. Parmaliana, N. Giordano, Appl. Catal. A 125 (1995) 39.
[14] R.G. Herman, Q. Sun, C. Shi, K. Klier, C.-B. Wang, W. Hu, I.E. Wachs, M.M. Bhasin, Catal. Today 37 (1997) 1.
[15] K. Otsuka, Y. Wang, I. Yamanaka, A. Morikawa, J. Chem. Soc., Faraday Trans. 89 (1993) 4225.
[16] V. Sokolovskii, Catal. Rev.-Sci. Eng. 32 (1990) 1.
[17] K. Yoshizawa, Y. Shiota, T. Yamabe, J. Am. Chem. Soc. 120 (1998) 564.
[18] K. Yoshizawa, Y. Shiota, T. Yamabe, Organometallics 17 (1998) 2825.
[19] F. Arena, F. Frusteri, A. Parmaliana, Appl. Catal. A 197 (2000) 239.
[20] F. Arena, F. Frusteri, A. Parmaliana, AIChE J. 46 (2000) 2285.
[21] F. Arena, F. Frusteri, A. Parmaliana, J. Catal. 207 (2002) 232.
[22] S. Yuen, J.E. Chen, J.A. Dumesic, N. Topsøe, H. Topsøe, J. Phys. Chem. 86 (1982) 3022.
[23] R. Joyner, M. Stockenhuber, J. Phys. Chem. B 103 (1999) 5963.

[24] K. Chen, Y. Fan, Z. Hu, Q. Yan, J. Solid. State Chem. 121 (1996) 240.
[25] X. Feng, W.K. Hall, J. Catal. 166 (1997) 368.
[26] L.A. Boot, A.J. van Dillen, J.W. Geus, F.R. van Buren, J. Catal. 163 (1996) 186.
[27] S. Bordiga, R. Buzzoni, F. Geobaldo, C. Lamberti, E. Giamello, A. Zecchina, G. Leofanti, G. Petrini, G. Tozzola, G. Vlaic, J. Catal. 158 (1996) 486.
[28] El-M. El-Malki, R.A. van Santen, W.M.H. Sachtler, J. Catal. 196 (2000) 212.
[29] G. Spoto, A. Zecchina, G. Berlier, S. Bordiga, M.G. Clerici, L. Basini, J. Mol. Catal. A 158 (2000) 107.
[30] P. Decyk, M. Trejda, J. Kujawa, K. Głaszczka, M. Bettahar, S. Monteverdi, M. Mercy, J. Catal. 219 (2003) 146.
[31] J. Jia, K.S. Pillai, W.M.H. Sachtler, J. Catal. 221 (2004) 119.
[32] S.-T. Wong, J.-F. Lee, S. Cheng, C.-Y. Mou, Appl. Catal. A 198 (2000) 115.
[33] G. Grosse, Mos90 (Version 2.2), Technical University of Munich (1992).
[34] F. Arena, A. Parmaliana, J. Phys. Chem. 100 (1996) 19994.
[35] F. Arena, F. Frusteri, G. Martra, S. Coluccia, A. Parmaliana, J. Chem. Soc., Faraday Trans. 93 (1997) 3849.
[36] F. Arena, N. Giordano, A. Parmaliana, J. Catal. 167 (1997) 66.
[37] L. Le Noc, D. Trong On, S. Solmykina, B. Echchahed, F. Beland, C. Cartier dit Moulin, L. Bonneviot, Stud. Surf. Sci. Catal. 101 (1996) 611.
[38] G. Lehmann, Z. Phys. Chem. Neue Folge 72 (1970) 279.
[39] L. Bonneviot, D. Trong On, A. Lopez, J. Chem. Soc., Chem. Commun. (1993) 685.
[40] L. Marchese, E. Gianotti, V. Dellarocca, T. Maschmeyer, F. Rey, S. Coluccia, J.M. Thomas, Phys. Chem. Chem. Phys. 1 (1999) 585.
[41] H.H. Tippins, Phys. Rev. B 1 (1970) 126.
[42] R. Bongiovanni, E. Pellizzetti, E. Borgarello, D. Meisel, La Chimica e l'Industria 4 (1994) 261.
[43] C.A. Brown, G.J. Remar, R.L. Musselman, E.I. Solomon, Inorg. Chem. 34 (1995) 688.
[44] E. Murad, J.H. Johnston, in: G.J. Long (Ed.), Mössbauer Spectroscopy Applied to Inorganic Chemistry, 1987, pp. 507–582.
[45] N.G. Gallegos, A.M. Alvarez, M.V. Cagnoli, J.F. Bengoa, S.G. Marchetti, R.C. Mercader, A.A. Yeramian, J. Catal. 161 (1996) 132.
[46] F. Arena, G. Gatti, G. Martra, S. Coluccia, A. Parmaliana, Catal. Today 91–92 (2004) 305.
[47] Q. Ma, K. Klier, H. Cheng, J.W. Mitchell, K.S. Hayes, J. Phys. Chem. B 104 (2000) 10618.
[48] P. D Maniar, A.J. Navrotsky, Non-Cryst. Solids 120 (1990) 20.
[49] Q. Sun, R.G. Herman, K. Klier, Catal. Lett. 16 (1992) 251.
[50] C.R.F. Lund, J.A. Dumesic, J. Phys. Chem. 85 (1981) 3175.
[51] J. Jia, J. Shen, L. Lin, Z. Xu, T. Zhang, D. Liang, React. Kinet. Catal. Lett. 64 (1998) 255.
[52] F. Arena, G. Gatti, S. Coluccia, G. Martra, A. Parmaliana, Stud. Surf. Sci. Catal. 147 (2004) 535.
[53] A. Bielañski, J. Haber, Oxygen in Catalysis, Dekker, New York, 1991.
[54] B.K. Hodnett, Heterogeneous Catalytic Oxidation, Wiley, New York, 2000.
[55] J.L. Callahan, R.K. Grasselli, AIChE J. 9 (1963) 755.
[56] R.K. Grasselli, Top. Catal. 15 (2001) 93.
[57] X. Feng, W.K. Hall, Catal. Lett. 41 (1996) 45.